A deep learning framework for light propagation modelling for quantitative photoacoustics

Mengjie Shi*, Tom Vercauteren, and Wenfeng Xia
Department of Biomedical Engineering and Imaging Sciences
King's College London
London, UK
*mengjie.shi@kcl.ac.uk

***Abstract*—Photoacoustic (PA) imaging is a hybrid modality based on optical absorption and ultrasound (US) detection. Quantitative PA imaging provides valuable functional information such as blood oxygen saturation, sO_2, by estimating chromophore concentrations from multispectral PA images. The quantification remains challenging due to unknown light attenuation in heterogeneous tissues. Monte Carlo (MC) simulation is regarded as the gold standard for modelling light propagation in turbid media. It leverages stochastic modelling methods through the simulation of the random walk of photon packets, thus it is computationally demanding and not suitable for real-time applications. In this work, for the first time, we propose a deep learning (DL) framework for light propagation modelling, with a focus on quantitative PA imaging. Compared to the MC simulation, our method reduced the computation time by 4 orders of magnitude, from 33 minutes to 46 milliseconds for a 3D simulation. In addition, the DL-based light fluence estimation improved sO_2 quantification accuracy, achieving an average estimation error of 0.3% with a blood phantom, and showed no significant difference compared to the MC simulation. This framework aims to provide a time-efficient solution for light propagation modelling in turbid media, thereby enhancing the quantification accuracy for real-time PA imaging applications.**

***Index Terms*—spectral decolouring, quantitative photoacoustic imaging, generative adversarial networks, oxygen saturation estimation**

I. Introduction

Photoacoustic (PA) imaging is an emerging modality that features a combination of optical spectroscopic contrast and ultrasonic spatial resolution [1]. Quantitative PA imaging provides functional and molecular information such as oxygen saturation (sO_2) by retrieving the relative concentrations of oxy- and deoxyhemoglobin in blood. However, accurate quantification remains challenging, especially for in vivo applications, due to the unknown wavelength-dependent light fluence distribution [2], [3]. While non-invasive assessment of light fluence distribution can be achieved with diffuse optical tomography and acousto-optics, it increases the system complexity and limits its practicability in clinical settings [4], [5]. Alternatively, the light fluence spectrum can be approximated using numerical methods that model light propagation in optical scattering and absorption media [6]. For example, Monte Carlo (MC) simulation is regarded as the gold standard for its accuracy and flexibility in terms of light propagation modelling [7]. MC method simulates the random walk of a photon as it propagates through turbid media, and tens to hundreds of millions of photon packets are typically required to ensure the convergence of absorbed energy density. The simulation process can be accelerated using graphical processing units (GPUs) [8] and parallelisation. Recent work also demonstrated the application of deep learning models for MC simulation acceleration by denoising the results acquired using a small number of photo packets [9]. However, the computational time required to obtain the noisy results was not alleviated, thereby limiting its suitability for real-time applications, such as guiding surgical and interventional procedures [10], [11].

Deep learning techniques, especially deep generative models, have garnered attention for their ability to produce high-fidelity synthetic images, particularly in the field of medical imaging, including representative applications such as retinal images [12], brain images [13], and dose radiation [14]. Our previous work showed the feasibility of applying conditional generative adversarial networks for light fluence synthesis and its application on light fluence compensation for quantitative PA imaging using simulated data [15]. In this work, we further extended the work by proposing a deep learning framework for light propagation modelling and validated its performance in terms of oxygen saturation estimation using phantom data.

II. Materials and Methods

A. Dataset preparation

The training data were prepared by simulating 3D light propagation in biological tissues using Monte Carlo eXtreme (MCX) [8]. The illumination patterns were modelled based on the PA probe used in the LED-based PA/Ultrasound (US) imaging system AcousticX where two LED bars were symmetrically positioned on either side of a linear array US probe, as shown in Fig. 1(a) [16]. A simulation domain of size 256 $\times$ 270 $\times$ 114 voxels was established with a spatial resolution of 0.1 mm. The two LED bars were simulated encompassing 38 $\times$ 2 (number of elements per row $\times$ number of rows) for each bar. The light incident from each LED element was simulated as a collimated Gaussian beam with a waist radius

This research was funded in whole, or in part, by the Wellcome Trust 203148/Z/16/Z, EPSRC NS/A000049/1, King's – China Scholarship Council PhD Scholarship program (K-CSC) and International Photoacoustic Standardisation Consortium (IPASC).

of 0.6 voxels (an opening angle of 120 deg). The spacing between the LED elements within the array was set to 0.7 mm, while the spacing between the distinct arrays was 1.25 mm. The ground truth by MC simulation was obtained using 10^8 photons. Fig. 1 demonstrates a 3D volumetric light fluence distribution and 2D light fluence distributions in the x-y, x-z, and z-y planes, respectively.

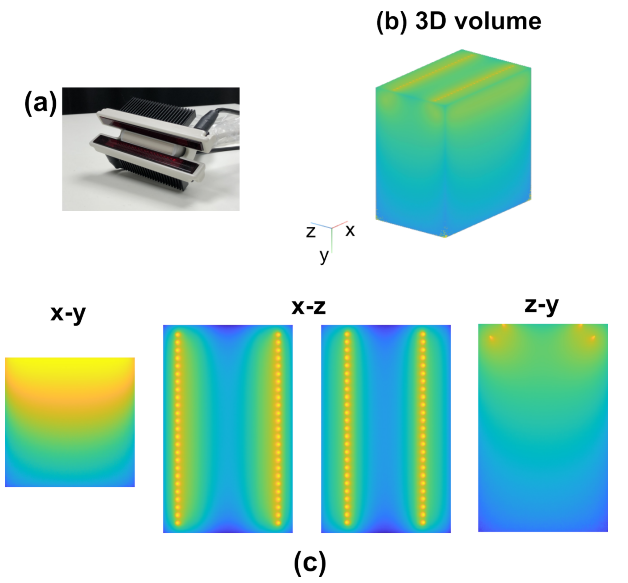

Fig. 1. Light fluence distribution in 3D acquired using Monte Carlo simulation. (a) Photography of an imaging probe used in a linear-array based photoacoustic/ultrasound imaging system with light-emitting-diode illumination. (b) Light fluence distribution in 3D (c) Light fluence distribution in 2D.

Furthermore, human soft tissue models were incorporated for light fluence simulation. The anatomical structures were derived from manual segmentations using in vivo human data based on co-registered US images acquired with the same probe. Fig. 2 shows a few representative tissue anatomies consisting of a coupling medium, a skin layer, and soft tissue. To augment the data, randomised deformations were introduced at the tissue boundaries (Fig. 2(c)). The parameterisation of the corresponding optical property maps was randomised according to the literature values of the tissue types in the wavelength range of 600 nm to 900 nm [17] (Tab. I). The tissue anatomical structure was defined in 2D and was stacked along the z-axis to obtain the tissue model in 3D. Finally, the light fluence distribution at the imaging plane (x-y) was extracted from the 3D light fluence volume. 800 samples with sizes of 256 $\times$ 256 were generated and used for model training.

B. Neural network implementation

A conditional generative adversarial network (cGAN) called pix2pix was employed for light fluence synthesis [18]. As shown in Fig. 3, the generator G took a multi-channel input comprising tissue segmentation maps encoded with three optical properties respectively, i.e., optical absorption coefficient μ_a, optical scattering coefficient μ_s, and anisotropy g. The generator G employed a UNET model architecture [19]. The

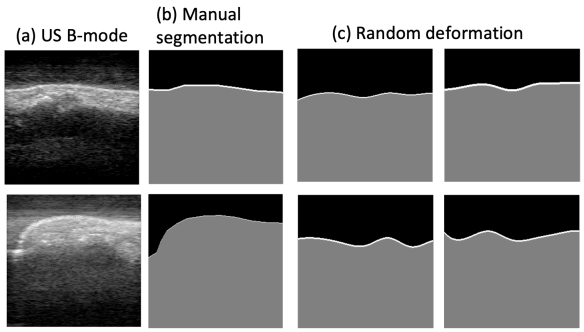

Fig. 2. Tissue anatomies used for Monte Carlo simulation. (a) B-mode Ultrasound (US) images of in vivo human fingers (up) and human wrist (bottom). (b) Manual segmentation using B-mode US images. (c) Random deformation at tissue boundaries.

TABLE I
OPTICAL PROPERTIES OF THREE TISSUE TYPES INVOLVED IN A HUMAN SOFT TISSUE MODEL (μ_a: OPTICAL ABSORPTION; μ_s: OPTICAL SCATTERING; g: GRUNEISEN PARAMETER; WAVELENGTH RANGE: 600 NM TO 900 NM)

	$\mu_a\ (\mathrm{mm}^{-1})$	$\mu_s\ (\mathrm{mm}^{-1})$	g
Coupling medium	[5e − 4 5e − 3]	[0.9 1]	1
Skin	[0.01 0.4]	[5 28]	0.9
Soft tissue	[0.001 0.13]	[7 12]	0.9

discriminator D was a PatchGAN network and trained to distinguish between light fluence maps generated from the generator G and MC method at the scale of patches. Here, a patch size of 16×16 was found to be effective.

C. Oxygen saturation estimation

Linear unmixing is the most commonly used method for blood oxygen saturation estimation using multispectral PA images. The multispectral PA images (initial pressure distributions) can be expressed as:

$$p_0(r,\lambda_i) = \Gamma\mu_a(r,\lambda_i)\phi(r,\lambda_i) \tag{1}$$

where Γ is Grüneisen parameter, μ_a is optical absorption cofficient, and ϕ is light fluence spectrum. Take blood oxygen saturation estimation as an example, μ_a can be written as the combination of oxyhemoglobin HbO_2 and deoxyhemoglobin HbR.

$$p_0(r,\lambda_i) = \Gamma\phi(r,\lambda_i)[C_{HbO_2}(r)\epsilon_{HbO_2}(\lambda_i)+C_{HbR}(r)\epsilon_{HbR}(\lambda_i)] \tag{2}$$

Suppose PA imaging is performed using two wavelengths λ_1 and λ_2, set

$$b(r,\lambda_i) = p_0(r,\lambda_i)/\Gamma\phi(r,\lambda_i) \tag{3}$$

Let A be:

$$A = \begin{bmatrix} \epsilon_{HbR}(\lambda_1) & \epsilon_{HbO_2}(\lambda_1) \\ \epsilon_{HbR}(\lambda_2) & \epsilon_{HbO_2}(\lambda_2) \end{bmatrix} \tag{4}$$

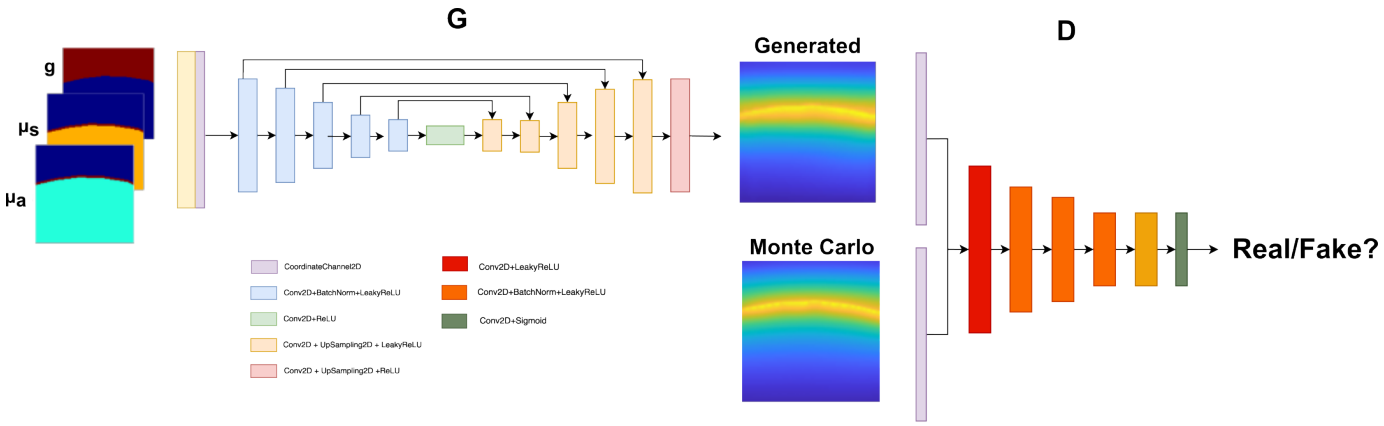

Fig. 3. A conditional generative adversarial network pix2pix for light propagation modelling in biological tissues. For the generator G, the input is an optical property-encoded segmentation based on ultrasound image and the output is a synthetic light fluence map. The discriminator D is trained to distinguish the real light fluence map generated by the Monte Carlo simulation and the synthetic light fluence map by the generator. μ_a: absorption coefficient, μ_s: scattering coefficient, g: Gruneisen parameter.

and the molar concentration of HbR and HbO_2 is:

$$x = \begin{bmatrix} C_{HbR}(r) \\ C_{HbO_2}(r) \end{bmatrix} \tag{5}$$

Eq. (2) can be expressed as a linear equation $Ax = b$ and the solution is given by:

$$x = (A^T A)^{-1} A^T b \tag{6}$$

Light fluence distribution $\phi(r, \lambda_i)$ in Eq. (3) is typically unknown and is assumed to be constant for linear unmixing. Therefore, light fluence compensation is necessary for accurate oxygen saturation estimation, with the light fluence distribution typically obtained using MC simulations.

D. Multispectral photoacoustic phantom

A multispectral PA phantom was developed for quantitative evaluation. Copper sulphate ($CuSO_4.5H_2O$) and nickel sulphate ($NiSO_4.6H_2O$) were selected as surrogates for HbO_2 and HbR [20]. 0.5 M copper sulphate mother solution and 2.2 M nickel sulphate mother solution were prepared and mixed following the ratiometric quantity defined in Eq. (7) where Q(%) is an analogue for oxygen saturation sO_2.

$$Q(\%) = \frac{\frac{c_{NiSO_4}}{2.2}}{\frac{c_{CuSO_4}}{0.5} + \frac{c_{NiSO_4}}{2.2}} \times 100 \tag{7}$$

The absorption coefficient spectra of the mixtures were measured by a Vis-NIR spectrophotometer (Aligent, CA, USA). The multispectral PA phantom comprised four silicone tubes, each with an inner diameter of 0.5 mm. These tubes were filled with mixtures of copper and nickel sulphate solutions, set against a background composed of 1% Intralipid and 0.0004% India ink. The imaging was conducted using the LED-based PA imaging probe encased within a cling film bag filled with water. For each mixture, both B-mode US data (1536 frames) and multispectral PA data (690 and 850 nm; 768 frames at each wavelength) were collected. Image reconstruction based on Fast Fourier Transform (FFT) [17] and PA quantification was conducted offline.

III. Results

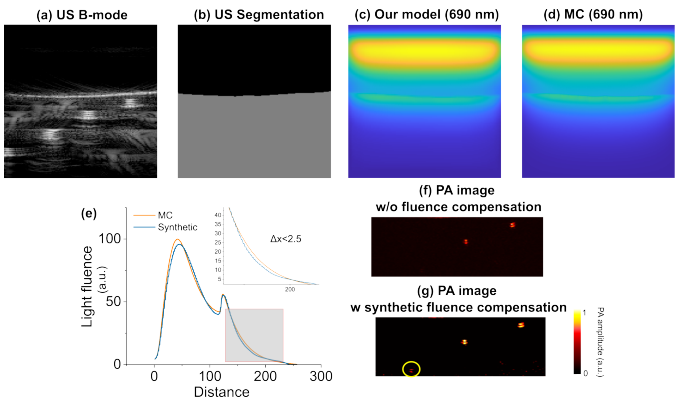

Fig. 4. Validation of the deep learning framework for quantitative photoacoustics (PA) using multispectral PA phantoms. (a) Ultrasound (US) image of the PA phantom. (b) Manual segmentation based on US contrast. (c) Light fluence map by pix2pix. (d) Reference light fluence map by Monte Carlo simulation. (e) Profiles comparing the light fluence decay in the depth direction. (f) Compensated and Uncompensated PA images.

The LED-based PA probe with LED arrays of two wavelengths (850 and 690 nm) was employed for imaging the multispectral PA phantoms. Fig. 4(a) is the US image of the phantom, showing the cling film separating the coupling medium and the aqueous background. Fig. 4(b) shows the corresponding US segmentation, with black representing the coupling medium and grey representing the background. Fig. 4(c-d) shows the light fluence maps generated by pix2pix and MC simulation at 690 nm. Besides, the light fluence distributions were further compared in Fig. 4(e) by drawing line profiles through the light fluence maps at the imaging plane. The maximum discrepancy between the synthetic light fluence map by pix2pix and the reference MC simulation was 2.5. In Fig. 4(f), PA signals from the tubes located at the deep depths were barely visible (indicated by a yellow circle). In contrast, the PA signals were enhanced by compensating

TABLE II
COMPARISON OF TIME EFFICIENCY IN LIGHT PROPAGATION MODELLING. MONTE CARLO (MC) SIMULATIONS WERE PERFORMED IN 3D WITH DIMENSIONS OF $256 \times 270 \times 114$ AND 10^8 PHOTONS.

	MC simulation	Our Model
Light fluence distribution at the imaging plane	33 mins	46 ms

The MC simulation and model tests were conducted using an NVIDIA QUADRO RTX 5000 GPU

the light attenuation estimated by pix2pix. Furthermore, the performance of the deep learning-based fluence compensation for PA spectral decolouring was validated using the phantom with a blood oxygenation level of 25%. The conventional linear unmixing method underestimated the oxygenation levels of the phantoms. The average sO_2 was around 22.1%. In contrast, the estimation accuracy was improved by incorporating light fluence distribution estimated by either pix2pix or MC simulation. The estimated sO_2 values were about 25.3% and 24.9% on average, respectively. There was no significant difference in terms of the estimated oxygenation obtained via pix2pix and MC simulation.

IV. DISCUSSIONS AND CONCLUSIONS

The primary challenge in achieving accurate quantitative PA imaging in biological tissues is the unknown light fluence. MC simulation, the gold standard for light propagation modelling, can approximate light fluence in the tissues. However, MC simulation can be computationally demanding, restricting its real-time applications in quantitative PA imaging. In this work, a deep learning framework was proposed for light propagation modelling in quantitative PA imaging. A deep generative model pix2pix was trained for generating light fluence distributions in heterogeneous tissues based on tissue anatomy and optical properties. Consequently, PA quantification such as sO_2 can be compensated using the estimated fluence spectrum. The proposed framework was validated using a liquid-based multispectral PA phantom that consisted of copper sulphate and nickel sulphate as surrogates for HbO_2 and HbR. High-quality light fluence spectra at 850 nm and 690 nm were generated by pix2pix, respectively, with the largest estimation error of around 2.5 compared to the fluence generated by the MC method, indicating the effectiveness of the deep learning-based fluence model. More importantly, the generated light spectrum was employed for light fluence compensation in PA quantification. Comparable estimation accuracy of sO_2 was achieved compared to the gold standard MC simulation. Moreover, the proposed model generated the light fluence distribution at the 2D imaging plane in under 46 ms, compared to around 33 mins using MC simulation (Tab. II). This significant improvement in computational efficiency enables the integration of light fluence compensation or iterative inversion methods for accurate and real-time quantitative PA imaging.

REFERENCES

[1] W. Xia, *Biomedical Photoacoustics: Technology and Applications*. Springer Nature, 2024.

[2] B. Cox, J. Laufer, and P. Beard, "The challenges for quantitative photoacoustic imaging," in *Photons Plus Ultrasound: Imaging and Sensing 2009*, vol. 7177, pp. 294–302, SPIE, 2009.

[3] A. Hauptmann and T. Tarvainen, "Model-based reconstructions for quantitative imaging in photoacoustic tomography," in *Biomedical Photoacoustics: Technology and Applications*, pp. 133–153, Springer, 2024.

[4] A. Q. Bauer, R. E. Nothdurft, T. N. Erpelding, L. V. Wang, and J. P. Culver, "Quantitative photoacoustic imaging: correcting for heterogeneous light fluence distributions using diffuse optical tomography," *Journal of biomedical optics*, vol. 16, no. 9, pp. 096016–096016, 2011.

[5] A. Hussain, W. Petersen, J. Staley, E. Hondebrink, and W. Steenbergen, "Quantitative blood oxygen saturation imaging using combined photoacoustics and acousto-optics," *Optics letters*, vol. 41, no. 8, pp. 1720–1723, 2016.

[6] B. Cox, J. G. Laufer, S. R. Arridge, and P. C. Beard, "Quantitative spectroscopic photoacoustic imaging: a review," *Journal of biomedical optics*, vol. 17, no. 6, pp. 061202–061202, 2012.

[7] L. Wang and S. L. Jacques, "Hybrid model of Monte Carlo simulation and diffusion theory for light reflectance by turbid media," *JOSA A*, vol. 10, no. 8, pp. 1746–1752, 1993.

[8] Q. Fang and D. A. Boas, "Monte carlo simulation of photon migration in 3d turbid media accelerated by graphics processing units," *Optics express*, vol. 17, no. 22, pp. 20178–20190, 2009.

[9] M. R. Ardakani, L. Yu, D. R. Kaeli, and Q. Fang, "Framework for Denoising Monte Carlo Photon Transport Simulations Using Deep Learning," p. 21.

[10] M. Shi, S. J. West, T. Vercauteren, S. Noimark, A. E. Desjardins, and W. Xia, "Photoacoustic imaging of interventional devices for guiding minimally invasive medical procedures," *Biomedical Photoacoustics: Technology and Applications*, pp. 547–571, 2024.

[11] W. Xia, M. Kuniyil Ajith Singh, E. Maneas, N. Sato, Y. Shigeta, T. Agano, S. Ourselin, S. J. West, and A. E. Desjardins, "Handheld real-time led-based photoacoustic and ultrasound imaging system for accurate visualization of clinical metal needles and superficial vasculature to guide minimally invasive procedures," *Sensors*, vol. 18, no. 5, p. 1394, 2018.

[12] P. Costa, A. Galdran, M. I. Meyer, M. Niemeijer, M. Abràmoff, A. M. Mendonça, and A. Campilho, "End-to-End Adversarial Retinal Image Synthesis," *IEEE Transactions on Medical Imaging*, vol. 37, no. 3, pp. 781–791, 2018.

[13] W. H. L. Pinaya, P.-D. Tudosiu, J. Dafflon, P. F. da Costa, V. Fernandez, P. Nachev, S. Ourselin, and M. J. Cardoso, "Brain Imaging Generation with Latent Diffusion Models," 2022.

[14] V. Kearney, J. W. Chan, T. Wang, A. Perry, M. Descovich, O. Morin, S. S. Yom, and T. D. Solberg, "DoseGAN: A generative adversarial network for synthetic dose prediction using attention-gated discrimination and generation," *Scientific Reports*, vol. 10, no. 1, p. 11073, 2020.

[15] M. Shi, T. Vercauteren, and W. Xia, "Learning to compensate spectral coloring in a led-based photoacoustic/ultrasound imaging system," in *Photons Plus Ultrasound: Imaging and Sensing 2024*, vol. 12842, pp. 69–72, SPIE, 2024.

[16] M. K. A. Singh, N. Sato, F. Ichihashi, W. Xia, and Y. Sankai, "The evolution of led-based photoacoustic imaging: From labs to clinics," in *Biomedical Photoacoustics: Technology and Applications*, pp. 573–608, Springer, 2024.

[17] S. L. Jacques, "Optical properties of biological tissues: a review," *Physics in Medicine & Biology*, vol. 58, no. 11, p. R37, 2013.

[18] P. Isola, J.-Y. Zhu, T. Zhou, and A. A. Efros, "Image-to-image translation with conditional adversarial networks," in *Proceedings of the IEEE conference on computer vision and pattern recognition*, pp. 1125–1134, 2017.

[19] O. Ronneberger, P. Fischer, and T. Brox, "U-net: Convolutional networks for biomedical image segmentation," in *Medical image computing and computer-assisted intervention–MICCAI 2015: 18th international conference, Munich, Germany, October 5-9, 2015, proceedings, part III 18*, pp. 234–241, Springer, 2015.

[20] M. B. Fonseca, L. An, and B. T. Cox, "Sulfates as chromophores for multiwavelength photoacoustic imaging phantoms," *Journal of Biomedical Optics*, vol. 22, no. 12, p. 125007, 2017.